ISPRS Journal of Photogrammetry and Remote Sensing 96 (2014) 224–235

Contents lists available at ScienceDirect

ISPRS Journal of Photogrammetry and Remote Sensing

journal homepage: www.elsevier.com/locate/isprsjprs

Review Article

An effective thin cloud removal procedure for visible remote sensing images

Huanfeng Shen [a], Huifang Li [a,*], Yan Qian [b], Liangpei Zhang [c], Qiangqiang Yuan [d]

[a] School of Resource and Environmental Sciences, Wuhan University, PR China
[b] Kunshan Bureau of Land and Resources, Jiangsu Province, PR China
[c] The State Key Laboratory of Information Engineering in Surveying, Mapping and Remote Sensing, Wuhan University, PR China
[d] School of Geodesy and Geomatics, Wuhan University, PR China

ARTICLE INFO

Article history:
Received 18 January 2014
Received in revised form 4 June 2014
Accepted 19 June 2014
Available online 1 September 2014

Keywords:
Thin cloud removal
High fidelity
Visible images
Adaptive
Homomorphic filter

ABSTRACT

Clouds are obstructions for land-surface observation, which result in the regional information being blurred or even lost. Thin clouds are transparent, and images of regions covered by thin clouds contain information about both the atmosphere and the ground. Therefore, thin cloud removal is a challenging task as the ground information is easily affected when the thin cloud removal is performed. An efficient and effective thin cloud removal method is proposed for visible remote sensing images in this paper, with the aim being to remove the thin clouds and also restore the ground information. Since thin cloud is considered as low-frequency information, the proposed method is based on the classic homomorphic filter and is executed in the frequency domain. The optimal cut-off frequency for each channel is determined semi-automatically. In order to preserve the clear pixels and ensure the high fidelity of the result, cloudy pixels are detected and handled separately. As a particular kind of low-frequency information, cloud-free water surfaces are specially treated and corrected. Since only cloudy pixels are involved in the calculation, the method is highly efficient and is suited for large remote sensing scenes. Scenes including different land-cover types were selected to validate the proposed method, and a comparison analysis with other methods was also performed. The experimental results confirm that the proposed method is effective in correcting thin cloud contaminated images while preserving the true spectral information.

1. Introduction

With the rapid development of earth observation technology, remote sensing images with different spatial, temporal, and spectral resolutions are now available. Most of these remotely observed images are affected by atmospheric conditions and climatic factors, such as clouds (Richter, 1996a,b; Richter et al., 2011). The channels with short wavelengths, such as the visible channels, are more sensitive to the atmospheric conditions than those channels with long wavelengths, such as the infrared channels (Li et al., 2012). For the study of the land surface, clouds are considered as a kind of contamination, which result in the ground information being weakened or even lost (Richter et al., 2011; Li et al., 2012). Therefore, thin cloud removal is an important way to improve the quality of remote sensing images.

Thin cloud removal is a challenging task since images of regions covered by thin clouds not only contain the cloud information but also the ground features, including the radiation and textures (Du et al., 2002; Li et al., 2012). This results in the ground features being directly influenced when the thin clouds are removed. The model-based absolute atmospheric correction methods are capable of eliminating the atmospheric attenuation if the knowledge of the sensor profile and the atmospheric properties are available and accurate (Jensen, 1996). However, the atmospheric properties are difficult to acquire, even when planned (Jensen, 1996; Liang, 2001). Moreover, it has been found that the model-based methods cannot handle the locally concentrated thin clouds effectively. Thus, some image-based methods for thin cloud removal in remote sensing images have been explored which are independent of the model and correct the radiation of cloudy pixels. According to the data source, the image-based methods can be divided into two categories: multi-image based methods and single-image based methods.

* Corresponding author.
E-mail address: l.hf@whu.edu.cn (H. Li).

http://dx.doi.org/10.1016/j.isprsjprs.2014.06.011
0924-2716/

The multi-image based methods correct the brightness of the cloudy pixels by fusing complementary information from other temporal or other sensor images (Du et al., 2002; Poggio et al., 2012). Taking the cloud-free image as the reference data, a number of fusion strategies have been used to correct the cloudy pixels. A direct and simple fusion strategy is to replace the cloudy pixels with the referenced clear pixels. However, there are some limitations to the multi-image based methods. First, the cloudy image should be positively related to the reference cloud-free images; if not, the fusion will lead to breaks or errors in the results. Second, the clouds in the multiple images should not cover the same region; otherwise, no complementary information can be used to restore the ground information. Third, geometric and radiometric calibrations are necessary preprocessings, and the calibration accuracy is directly related to the final fusion result. Overall, the multi-image based thin cloud removal methods have strict requirements for data, which limits their application.

In contrast, the single-image based methods are independent of the referenced data, so their applications are broad. Several image enhancement methods have been used to restore the ground information under thin clouds, of which histogram matching has been the most widely used method (Stockham, 1972; Schreiber, 1978; Fries and Modestino, 1979). A typical image-based atmospheric correction method is the dark object subtraction (DOS) method, which treats all pixels equally (Chavez, 1988; Zhang et al., 2002). However, clouds are accumulations of liquid droplets or other particles suspended in the atmosphere, and are locally distributed rather than globally. Thus, DOS is capable of eliminating the influence of the global path radiation but fails to remove local thin clouds. Therefore, a level-based DOS method for thin cloud removal has also been developed, which segments the haze/cloud into several levels through haze optimized transformation (HOT) before the correction (Zhang et al., 2002). HOT is designed for the detection and characterization of haze/cloud distributions in Landsat scenes. It is a supervised procedure which requires cloudless samples to construct the clear-sky line. Thus, the results of HOT depend on the selection of cloudless samples from the cloudy scenes. Advanced HOT has also been developed to overcome land-cover confusion by introducing spatial constraints, but it still depends on the sample selection (He et al., 2010). Researchers have also tried to apply variational image processing methods to remote sensing images, but these methods are too complicated to handle the large scenes (Lan et al., 2013). All the above methods are operated in the spatial domain, but some methods that are operated in the frequency domain (with high computational efficiency) have also been developed. Thin clouds occupy the low-frequency parts of the image in the frequency domain, and can be extracted by a reasonable low-pass filter. Wavelet analysis (WA) (Du et al., 2002) and the homomorphic filter (HF) (Stockham, 1972; Schreiber, 1978; Fries and Modestino, 1979; Liu and Hunt, 1984) have both been utilized for thin cloud removal. WA involves the choice of wavelet basis, which is complicated, whereas the HF procedure is direct and clear. Moreover, the basic assumption of the HF can be used to model a cloudy image. However, the traditional HF is a global operation, which means that the brightness of both clear and cloudy pixels will be changed. This often leads to serious radiometric distortion in the results.

The existing methods are either complicated or not effective enough for the removal of locally aggregated thin clouds. In this paper, a simple but highly efficient and effective method that is based on the HF is proposed for the removal of thin clouds in visible remote sensing images. We intend to preserve the original radiometric DN values outside of haze areas in the multispectral image while removing the atmospheric scattering effects. This paper is organized as follows: Section 2 describes the HF and its use in thin cloud removal. The thin cloud removal method based on the HF is developed and the details are presented in Section 3. Several Landsat and high spatial resolution images are used in the experiments in Section 4. Section 5 concludes the paper.

2. Use of the homomorphic filter for thin cloud removal

Generally, the observed remotely sensed image $f(x, y)$ consists of two radiation components, namely the reflected component $R(x, y)$ and scattered component $S(x, y)$, in which the scattered component is also named as the path radiance (Vermote et al., 1997; Liang, 2001; Perkins et al., 2012). Thus, the observed image can be expressed as $f(x, y) = R(x, y) + S(x, y)$. It should be mentioned that the path radiance is neglected in the presented method and the effect of the thin cloud is attributed to the transmittance of the atmosphere. Therefore, the observing model can be written as follows, which is also the basic assumption of the HF.

$$f(x,y) = i(x,y) \cdot r(x,y) \tag{1}$$

where $i(x, y)$ represents the illumination component, which is distributed in the low frequency; and $r(x, y)$ represents the reflection component, which is distributed in the high frequency. Thus, the illumination and reflection components can be estimated by low-pass and high-pass filters in the frequency domain.

Thin clouds are mainly generated by the atmospheric scattering of large particles, including dust, smoke, and water droplets (Du et al., 2002). The spatial distributions of thin clouds are locally aggregated and continuous over the land surface. Therefore, thin clouds are usually assumed to locate in the low frequency of a cloudy image (Liu and Hunt, 1984; Du et al., 2002). It is possible to remove thin clouds by suppressing the low-frequency information while enhancing the high-frequency information. The universal procedure of the HF for thin cloud removal is described in Algorithm 1.

Algorithm 1. Thin cloud removal via the homomorphic filter

Input: observed image $f(x, y)$.
Logarithm: $z(x, y) = \ln f(x, y) = \ln i(x, y) + \ln r(x, y)$.
Fourier transformation:
$\mathcal{F}\{z(x,y)\} = \mathcal{F}\{\ln i(x,y)\} + \mathcal{F}\{\ln r(x,y)\}$, simplified as:
$Z(u, v) = F_i(u, v) + F_r(u, v)$,
where $F_i(u, v)$ and $F_r(u, v)$ represent the Fourier transformation of $\ln i(x, y)$ and $\ln r(x, y)$.
Filtering: use filter $H(u, v)$ to suppress the low-frequency information including the thin clouds, and meanwhile enhance the high-frequency information including the land cover:
$S(u, v) = H(u, v)Z(u, v) = H(u, v)F_i(u, v) + H(u, v)F_r(u, v)$.
Inverse Fourier transformation: $s(x,y) = \mathcal{F}^{-1}\{S(u, v)\}$.
Exponent: $g(x, y) = \exp[s(x, y)]$.
Alternative step: keep the dynamic range of the output consistent with that of the input by linear stretching:

$$g_L(x,y) = a_0 + \frac{b_0 - a_0}{b - a}(g(x,y) - a) \tag{2}$$

where $[a_0, b_0]$ is the dynamic range of the input, and $[a, b]$ is the dynamic range of $g(x, y)$.
Output: filtered image $g_L(x, y)$.

The HF is an unsupervised and efficient method for thin cloud removal. The cut-off frequency, which is used to separate the high and the low frequencies, is needed in the filter $H(u, v)$. Because the disturbance of clouds depends on the channel wavelength, the

cut-off frequency should vary with the wavelengths of the different channels. Thus, the cut-off frequency is a channel-dependent variable and is difficult to determine. Moreover, it is directly related to the thin cloud removal results.

The radiation values of all the pixels, both cloudy and cloudless, are modified after the operation of the HF. This whole-scene computation not only increases the computational burden but also destroys the spectral features of the cloudless pixels, no matter whether they are distributed in the high or low frequency. Specifically, if the cloudless land cover has a big spatial variation, its brightness is enhanced in the HF result. Conversely, if the cloudless land cover is spatially stable, its brightness is suppressed in the HF result. Consequently, it is reasonable to investigate a local thin cloud removal method which can retain the information of the cloudless land cover in the low frequency while removing the thin clouds.

3. Proposed methodology

To overcome the shortcomings of the traditional HF method, a high-fidelity thin cloud removal method based on the HF is proposed and described in this section. Three stages are included in the proposed method, as shown in the flowchart in Fig. 1: the cut-off frequency decision, the thin cloud removal, and the mosaicking of the cloudy and cloud-free sub-images. In the first stage, the cut-off frequency D of each channel is determined semi-automatically based on the relationship between the frequency and the gradient G, i.e. the product of D and G is a constant C. In the second stage, the thin clouds are first detected, and then the high-fidelity thin cloud removal method is performed to eliminate the disturbance of the thin clouds while retaining the cloudless pixels. It should be noted that the cloudy image is usually partially covered by clouds. The above two stages, frequency decision and thin cloud removal, are both operated on the cloudy subsets of the whole scene, and the cloudless parts are reserved in the results. Therefore, the mosaicking of the sub-images is performed in the final stage. In the result, the radiations of the cloudy land covers are corrected and the cloud free ones are restored.

3.1. Cut-off frequency decision

The HF can be used for thin cloud removal as the thin cloud is usually distributed in the low frequency. A cloud-free result can be expected by enhancing the information in the high frequency while suppressing the information in the low frequency. However, some land cover can vary slowly, in the same way as the thin cloud in the low frequency. If the cut-off frequency is too low, the high-pass filter cannot filter out all the low-frequency components, which means that part of the thin clouds will be left in the image. Otherwise, if the cut-off frequency is too high, information about some clear land cover will be filtered out. The cut-off frequency therefore has a great influence on the result, and how to determine an appropriate cut-off frequency is a difficult problem.

As mentioned before, the effect of thin clouds on the image is channel dependent because the atmospheric interference varies with the radiometric wavelength. The shorter the wavelength is, the stronger the atmospheric scattering is, and the higher the cut-off frequency should be. Thin clouds are more obvious in the visible channels than in the infrared channels, so that only visible channels are concerned and treated in this paper. A semi-automatic cut-off frequency decision method is introduced in this section by investigating the variation in the cut-off frequency between the channels. Here, semi-automatic means that for multispectral images, once the cut-off frequency for one channel is determined, the others can be fixed by considering the correlations between the channels. In the proposed method, the cut-off frequency for the blue channel is chosen to be first determined.

In general, thin clouds cause two changes in visible images: high brightness and a low gradient. On the one hand, the brightness is directly related to the land cover and is variable. If the underlying surface of the cloud has a high reflectance, the cloudy pixels are bright; otherwise, the brightness of the cloudy pixels

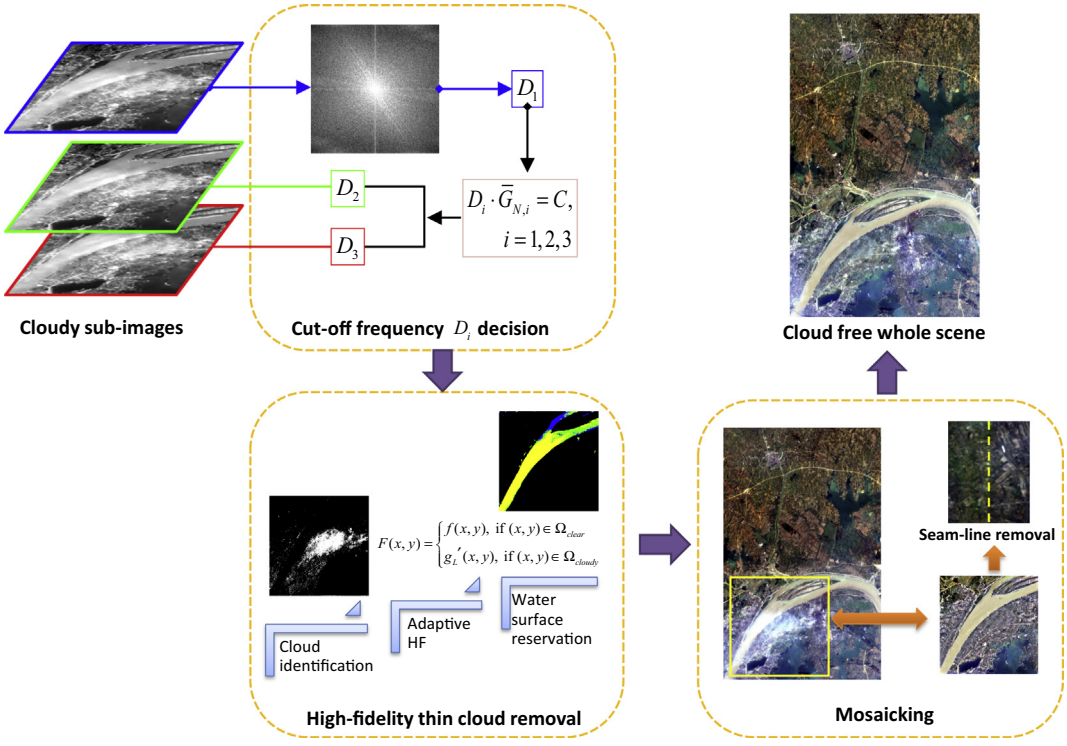

Fig. 1. Flowchart of the proposed thin cloud removal method.

may be close to that of some of the bright and cloudless pixels. On the other hand, the gradient is a relative concept which is more stable than the brightness. The difference between the gradient of a bright surface and a dark surface is not as evident as that of the brightness, which means that a low gradient can be attributed to thin clouds. Here, the gradient is represented by the average gradient $\bar{G}$ of an image, which can be expressed as:

$$\bar{G}_i = \frac{1}{(M-1)(N-1)} \sum_{x=1}^{M-1} \sum_{y=1}^{N-1} \sqrt{\frac{(F_i(x,y)-F_i(x+1,y))^2 + (F_i(x,y)-F_i(x,y+1))^2}{2}} \times (i=1,2,3) \quad (3)$$

M and N are the width and height of the image, and $F_i(x, y)$ represents the DN value of the pixel in the ith channel located at (x, y).

Considering a multispectral cloudy image, due to the variation in the atmospheric effect among the channels, the average gradient is positively related to the wavelength, and the cut-off frequency is negatively related to the wavelength. This suggests that the cut-off frequency is negatively related to the average gradient. Thus, we intend to explore the relationship between the cut-off frequency and the average gradient of the cloudy image in each channel. In order to investigate the quantitative relationship between D and $\bar{G}$ in a multispectral image, experiments were performed on a large amount of cloudy Landsat data and some GaoFen-1 data (2 meters spatial resolution). Taking Landsat data for example, the color image of a cloudy scene and the three visible bands of the scene, i.e. ETM 1 (central wavelength 0.48 μm), ETM 2 (0.56 μm), and ETM 3 (0.66 μm), are shown in Fig. 2. It is clear that with the increase in the wavelength, the influence of the thin clouds decreases so that the details, including edges and textures, increase. The gradient of each channel is related to the dynamic range of the corresponding channel. To ensure the comparability of the different gradients, the average gradient of each channel is normalized by multiplying by a coefficient, which is equal to the brightness ratio. Here, the brightness of each channel is represented by the average DN value in this channel. Specifically, for the visible image composed of ETM1, ETM2, and ETM3, ETM1 is taken as the reference image, and the brightness ratio is taken as the normalizing factor. Suppose the brightness of the processed image is B_i, and the brightness of the reference image is B_r. The brightness ratio is defined as the ratio of B_i to B_r. Therefore, the normalized average gradient can be expressed as:

$$\bar{G}_{N,i} = \frac{B_r}{B_i} \cdot \bar{G}_i \ (i = 1,2,3) \quad (4)$$

The normalized gradients of each channel, calculated by referencing with the first channel ETM1, are calculated and listed in Table 1. The optimal cut-off frequency for each channel, determined by manual tuning, is also listed in Table 1. The last column of Table 1 shows the products of the optimal cut-off frequency D and the normalized average gradient $\bar{G}_N$. It is found that for a multispectral image, the products of D and $\bar{G}_N$ are approximately constant for the three visible channels, i.e.

$$D_1 \cdot \bar{G}_{N,1} \approx D_2 \cdot \bar{G}_{N,2} \approx D_3 \cdot \bar{G}_{N,3} = C \quad (5)$$

Once the constant C is determined, the optimal cut-off frequency for each channel can be estimated. In practice, the first channel is taken as the reference channel, whose optimal cut-off frequency needs to be first determined by manual tuning. The constant can be obtained by the product of D_1 and $\bar{G}_{N,1}$, and then the cut-off frequencies of the other channels can be estimated by dividing C by the average gradient $\bar{G}_N$ of the corresponding channel. It is therefore a semi-automatic cut-off frequency decision method, the effect of which will be further evaluated in the following experiments.

3.2. High-fidelity thin cloud removal

To overcome the shortcomings of the traditional global HF, an adaptive HF is proposed, and water surfaces with large areas are isolated for special treatment. Specifically, to ensure the high fidelity of the result, three steps are included in this stage: cloud identification, the adaptive HF, and water surface identification and correction. It is noted that the proposed method is limited to treat the scenes with thin clouds, as the ground information weakened by thin clouds can be enhanced, but no information is under the thick clouds.

3.2.1. Thin cloud identification

The traditional HF is a kind of global operation, which changes the values of all the pixels, no matter they are cloudy or not. However, the values of cloudless pixels should be preserved for a high-fidelity thin cloud removal method. Thus, a thin cloud identification procedure is embodied in our proposed method. Several thin cloud identification methods have been reported in the literature, which can be divided into two categories: the threshold-based methods (Ackerman et al., 1998; Le Hégarat-Mascle and André, 2009) and the transformation-based methods (Zhang et al., 2002; Li et al., 2014). All of these methods involve several empirical parameters, which are related to the processed data. Furthermore, these methods are executed in the spatial domain, which is independent of our proposed procedure in the frequency domain. Therefore, in order to construct a uniform framework, a simple cloud identification method utilizing the property of the HF is introduced in our procedure.

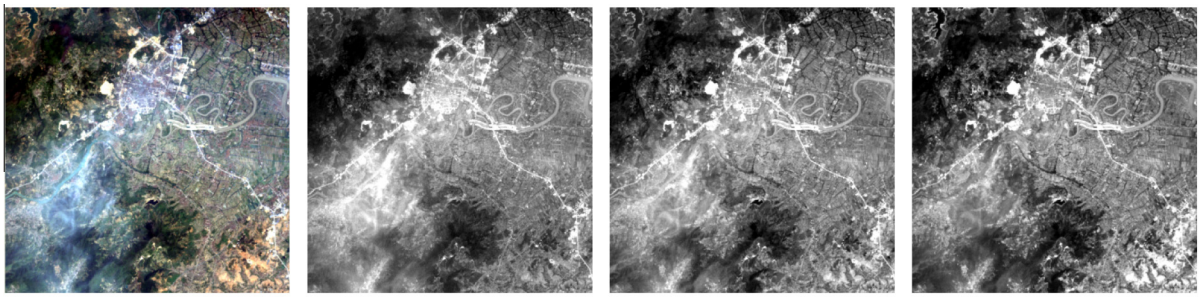

Fig. 2. The color image of a cloudy scene and the three monochromatic images in the visible channels. (a) The color image. (b) The image in the blue channel. (c) The image in the green channel. (d) The image in the red channel. (For interpretation of the references to colour in this figure legend, the reader is referred to the web version of this article.)

Table 1
The optimal cut-off frequencies D and normalized average gradients $\bar{G}_N$ of the four multispectral images.

		D	$\bar{G}_N$	$D \cdot \bar{G}_N = C$
Image 1	Band 1	13	2.669	34.697
	Band 2	10	3.666	36.66
	Band 3	6	5.812	34.872
Image 2	Band 1	20	1.688	33.76
	Band 2	16	2.088	33.408
	Band 3	11	3.307	36.377
Image 3	Band 1	15	1.475	22.125
	Band 2	11	1.844	20.284
	Band 3	7	3.124	21.868
Image 4	Band 1	8	1.704	13.632
	Band 2	6	2.389	14.334
	Band 3	3	4.132	12.396

Since the high-frequency information is enhanced and the low-frequency information is weakened after the HF, the values of pixels distributed in the low frequency will be lower than before, and the values of the other pixels will be higher than before. Thus, the cloudy pixels will have lower values after being processed, while the cloudless pixels will have higher values than before.

Suppose $e(x, y)$ represents the difference between the original pixel value $f(x, y)$ and the calculated pixel value $g_L(x, y)$ of the HF at location (x, y), i.e. $e(x, y) = f(x, y) - g_L(x, y)$. Based on the above analysis, if $e(x, y) > 0$, the pixel located at (x, y) is cloudy; otherwise, it is cloudless. This cloud identification is a pixel by pixel operation without considering the neighbors, which will result in some outliers. Hence, with regard to the continuity of the cloud, a window template, as shown in Fig. 3, is used to optimize the cloud identification. If the difference is negative for the central pixel (x_0, y_0) and positive for the eight pixels in the neighborhood, the central pixel will be identified as cloudy. Hence, a spatially continuous cloud map with cloudy and cloudless labels is obtained.

3.2.2. The adaptive homomorphic filter (HF)

Based on the identified cloud map, the cloudless pixels are assigned the original values f and the cloudy pixels are assigned the results g, as calculated by the HF. The overall procedure can be expressed as:

$$F(x,y) = \begin{cases} f(x,y), & \text{if } (x,y) \in \Omega_{cloudless} \\ g(x,y), & \text{if } (x,y) \in \Omega_{cloudy} \end{cases} \quad (6)$$

where F represents the final value, and $\Omega_{cloudless}$ and Ω_{cloudy} represent the clear and cloudy pixel sets, respectively. It is an adaptive operation, varying according to the property of the pixel. In this way, the precision of the thin cloud removal result is ensured by preserving the radiation values of the cloudless pixels distributed in the high frequency.

In the traditional HF procedure, there is an alternative step, linear stretching, which aims to keep the dynamic range of the output consistent with that of the input. Commonly, the dynamic range of the input is based on the statistics of all the cloudy and cloudless pixels in an image. However, with the interference of thin clouds, the maximum of the input is probably the value of some of the cloudy pixels. Therefore, after the cloud map is obtained, the statistics, including maximum and minimum, should be calculated based on the cloudless pixels. Moreover, pixels with the top 2% maximum and minimum values are excluded from the statistics to avoid the effect of outliers. In this way, the new target dynamic range is close to the cloudless land-surface truth. The linear stretching, using the new target dynamic range, is performed on the cloudy pixels, and the new output is $g'_L(x, y)$. Hence, the final thin cloud removal result can be written as:

$$F(x,y) = \begin{cases} f(x,y), & \text{if } (x,y) \in \Omega_{clear} \\ g'_L(x,y), & \text{if } (x,y) \in \Omega_{cloudy} \end{cases} \quad (7)$$

3.2.3. Water surface identification and correction

There can be cloudless and homogeneous regions with large areas in a scene, whose values will also be decreased by the HF, as well as the cloudy pixels. The pixels in this kind of region can be wrongly sorted into the cloudy category. A typical homogeneous region is a water surface such as a lake or a river. According to the physical property of water, if the water is clean with few suspended substances, the radiation is low; otherwise, if the water is turbid and full of suspended substances, the radiation is high. The radiation decrease caused by the HF has only a slight influence on clean water. This is because clean water usually has the lowest radiation in a scene, and the final brightness can be kept consistent with that of the input by linear stretching. However, the radiation decrease has a large impact for turbid water, because it changes the distribution of the turbid water in the radiation dynamic range. This will cause serious radiometric distortion of the water surface in the scene. Therefore, a step is introduced to detect the surface of turbid water, and then the radiation values of cloudy pixels on the water surface are specially treated.

(a) Water surface identification

A supervised classification is proposed to separate the turbid water and the other surfaces. Since the direction of the spectral vector is not sensitive to the clouds, the spectral angle is taken as the distance measure for the classification (Maselli et al., 2009). The types of classes vary according to the situation of the land cover. The turbid water class must be included, and the other classes should be determined with regard to the scene. The spectral angles between the unknown pixels and the class centers are calculated, and the unknown pixels belong to the class between which the spectral angle is the smallest. Hence, the surface of the turbid water is marked in the cloudy scene. Moreover, it is noted that cloudy and clear pixels coexist on the water surface. In order to preserve the radiation values of clear pixels to the greatest degree, the clear and cloudy pixels are distinguished before the treatment of the water surface is performed. For a smooth water surface, the high brightness is an evident characteristic for the

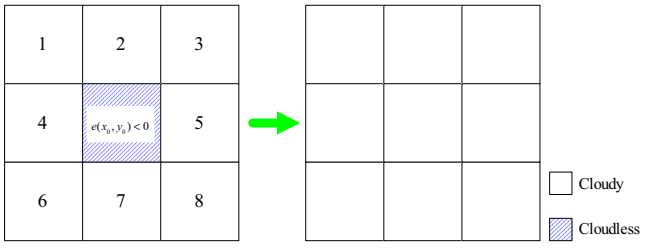

Fig. 3. The template used to ensure the continuity of the cloud.

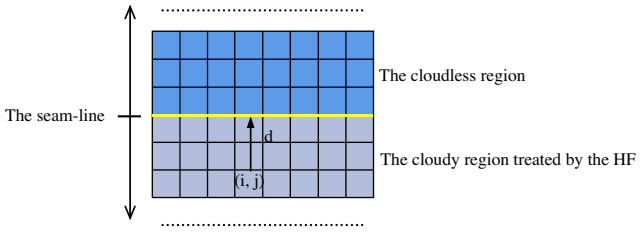

Fig. 4. An example of a horizontal seam-line.

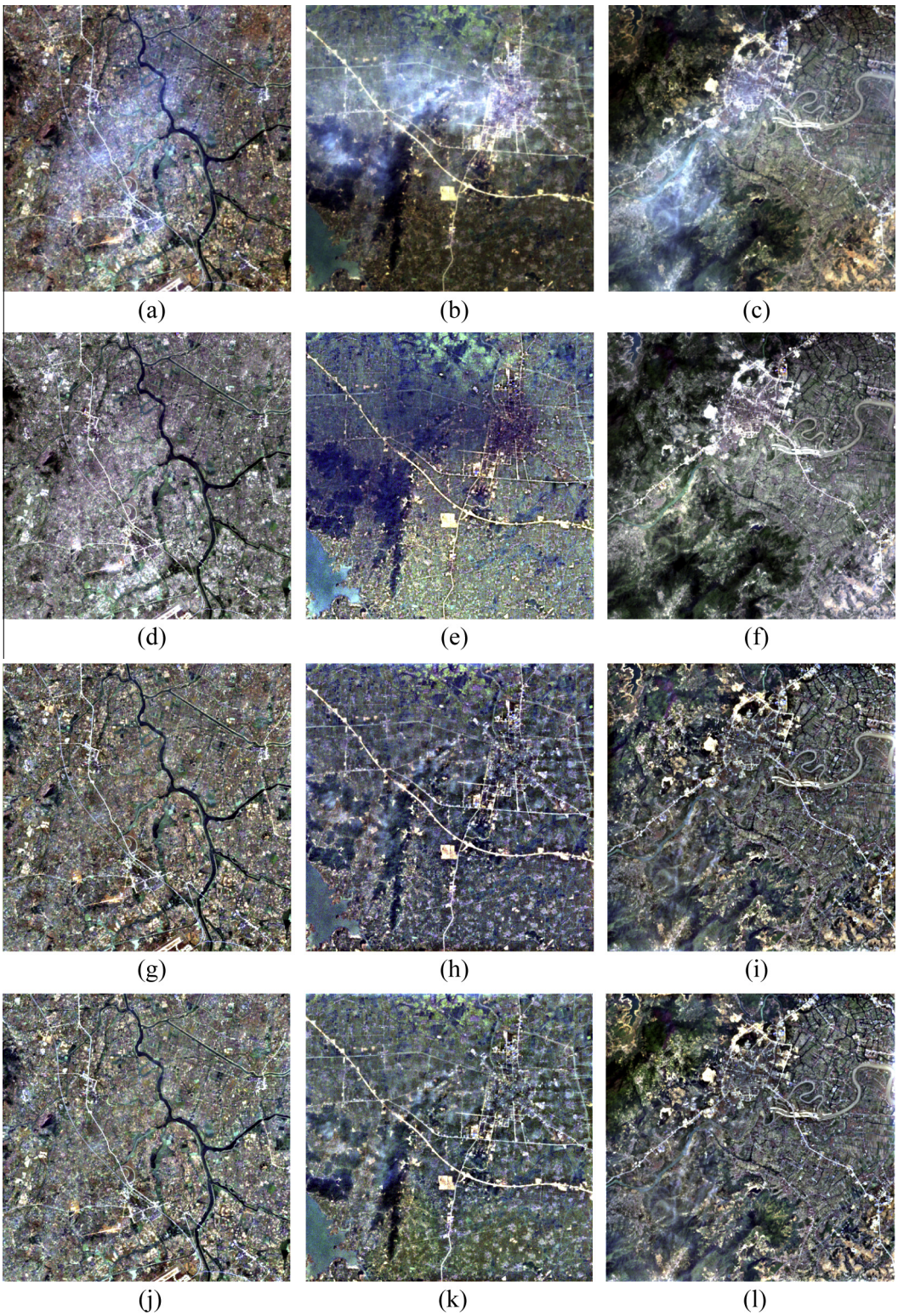

Fig. 5. Thin cloud removal results of the three images. The first row shows the original three images covered by thin clouds. The second row shows the results of HOT. The third row shows the results of the traditional HF. The fourth row shows the results of the adaptive HF.

cloudy pixels. Suppose that in the ith channel, the mean brightness of the clear water samples is $\overline{DN}_{W,i}$ and the value of an unknown pixel is DN_i. If $DN_i > \overline{DN}_{W,i}$ in all the channels, the pixel is labeled as cloudy; if $DN_i \leqslant \overline{DN}_{W,i}$ in all the channels, the pixel is labeled as clear; otherwise, the pixel is labeled as uncertain. Different treatments will be executed on these water pixels belonging to the three different classes.

(b) Water surface correction

Smooth water surfaces are specially treated, as the HF always decreases the brightness of the regions with low contrast. Since the water surfaces are grouped into three classes, clear, cloudy, and uncertain, in the final step, treatments are made according to the pixel type.

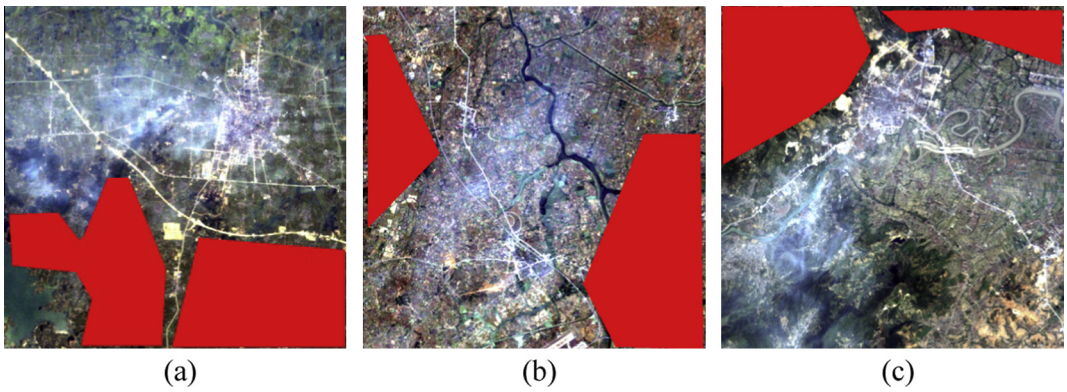

Fig. 6. Clear samples selected from the three images.

Table 2
Factor R of the different results.

		HOT	HF	Adaptive HF
Image 1	Band 1	1.0701	0.6511	0.6476
	Band 2	0.8415	0.9531	0.7116
	Band 3	0.6031	1.4849	0.4763
Image 2	Band 1	2.1786	2.3623	0.3107
	Band 2	2.2071	1.6114	0.3978
	Band 3	2.9156	1.7205	0.9646
Image 3	Band 1	3.7673	6.0502	0.4953
	Band 2	2.8004	5.2707	0.6793
	Band 3	2.8957	7.3697	0.6854

For the clear pixels, the original brightness is preserved to ensure the quality of the final result.

For the cloudy pixels, we use moment matching (Gadallah et al., 2000; Daniel et al., 2004) to correct the brightness. The moment matching method is suitable for regions with uniformly distributed radiation. By making use of the statistical information, the distribution of the cloudy pixels can be adjusted to that of the reference clear pixels by the following expression:

$$DN'_{W,i} = \frac{\sigma'_i}{\sigma_i}(DN_{W,i} - \mu_i) + \mu'_i \tag{8}$$

where $DN'_{W,i}$ is the corrected DN of the target pixel in the ith channel, μ_i and σ_i are the mean and standard deviation of the cloudy pixels, and μ'_i and σ'_i are the mean and standard deviation of the clear water samples.

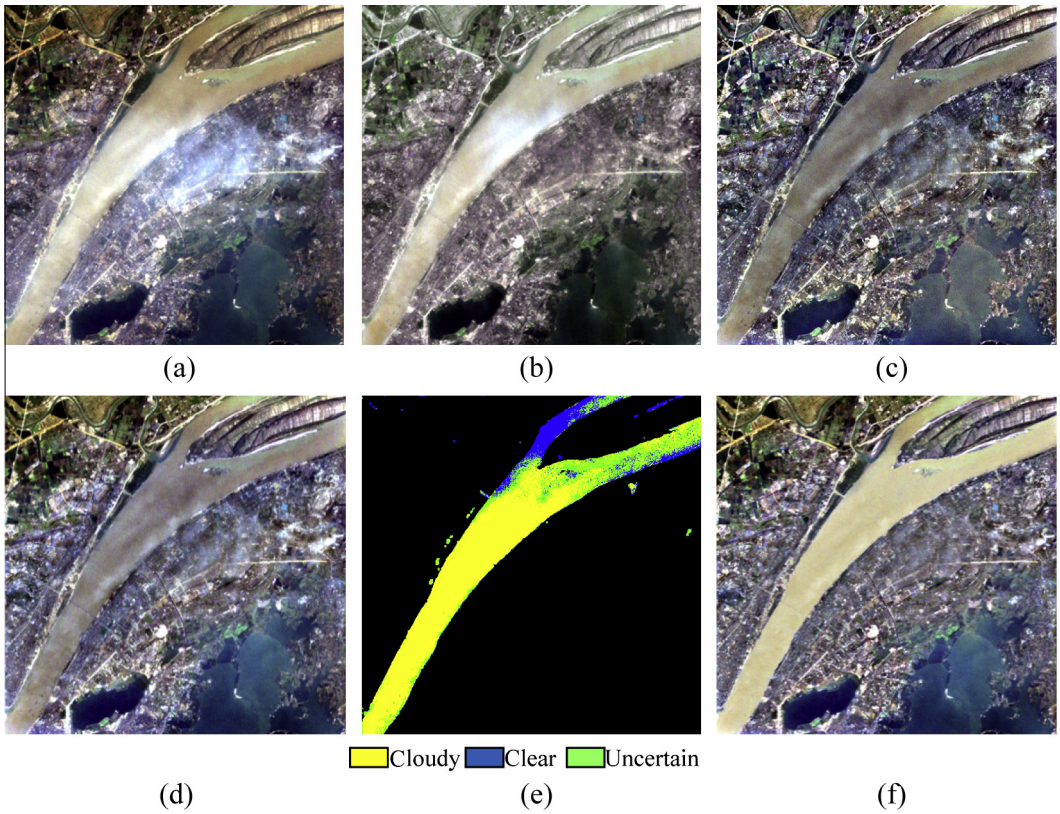

Fig. 7. The first image, including a large area of water surface, and the corresponding thin cloud removal results of the different methods. (a) The original image. (b) HOT. (c) Traditional HF. (d) Adaptive HF. (e) Class map of the water surface composed of the three classes. (f) The proposed method with water surface preservation.

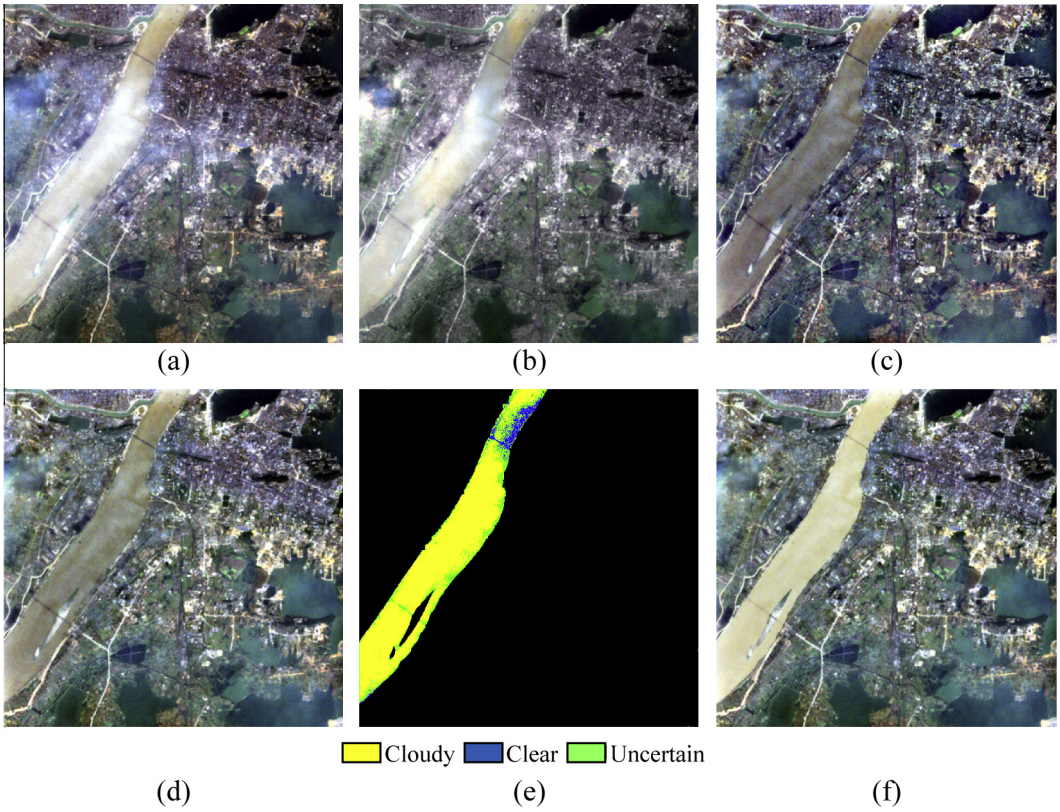

Fig. 8. The second image, including a large area of water surface, and the corresponding thin cloud removal results of the different methods. (a) The original image. (b) HOT. (c) Traditional HF. (d) Adaptive HF. (e) Class map of the water surface composed of the three classes. (f) The proposed method with water surface preservation.

For the uncertain pixels, the output brightness is the weighted sum of the original brightness $DN_{W,i}$ and the corrected brightness $DN'_{W,i}$, which can be written as:

$$F_{W,i} = t \cdot DN_{W,i} + (1 - t) \cdot DN'_{W,i} \tag{9}$$

where t is used to balance $DN_{W,i}$ and $DN'_{W,i}$. Suppose the multispectral image has N channels. If the condition $DN_i \leqslant \overline{DN}_{W,i}$ is satisfied in n ($n \leqslant N$) channels, $t = n/N$. It can be seen that the operations on clear and cloudy pixels are special situations of Eq. (9). When the pixel is clear, $t = 1$; when the pixel is cloudy, $t = 0$.

Hence, the brightness decrease caused by the HF is avoided and the brightness of the pixels on turbid water surfaces is preserved.

3.3. Mosaicking of the cloudy and cloud-free sub-images

In practice, thin clouds are usually concentrated in a local area, instead of covering the whole scene. Relative to the whole scene, parts of the scene are defined as sub-images. To improve the calculation efficiency and to reduce the information loss, the correction is only performed on the sub-images with thin clouds, and the other cloud-free sub-images are retained. The corrected sub-images replace the cloudy sub-images by mosaicking back to the whole image. Because the processing only involves some of the pixels of the whole scene, it is highly efficient and is capable of handling large cloudy scenes. However, it is inevitable that obvious seam-lines appear near the boundaries of the sub-images because the brightness of the cloudy image is changed. These seam-lines should be removed to ensure a smooth transition from the cloudy sub-images to the cloud-free sub-images.

In general, the brightness of pixels near the boundaries of the cloudy sub-images is adjusted to remove the seam-lines. Specifically, for one cloudy sub-image, there are four seam-lines, two vertical lines, and two horizontal lines. If the seam-line is vertical, the adjustment direction is horizontal; otherwise, the adjustment direction should be vertical. Fig. 4 shows an example of a horizontal seam-line.

The adjustment width L is set to determine which pixels need adjustment, which is tuned manually in our experiments. All the pixels with distances to the seam-lines less than L are adjusted and the others are kept constant. Taking Fig. 4 as an example, the distance of the pixel located at (x, y) to the seam-line is d, and $d \leqslant L$. Because no seam-line exists in the original whole image, the adjustment integrates both the original and the corrected values of the pixels. Specifically, the further the pixel is from the seam-line, the closer the value of the pixel should be to the corrected value; otherwise, it should be closer to the original vale. The values of the pixels located within the adjustment width can be calculated as follows:

$$F_M = \lambda f + (1 - \lambda)F \tag{10}$$

where $\lambda = d/L$ is used to weight the contribution of the corrected value in the final result. Processing the four seam-lines in the same way, the cloudy sub-images are mosaicked to the large whole scene without artifacts. Cloud-free large images with a high fidelity can then be obtained.

4. Experiments

Since thin clouds are sensitive to the wavelength, five thin cloudy visible images obtained by Landsat ETM+ and two by GaoFen-1 were employed to test the proposed thin cloud removal method. Three of the Landsat data and GaoFen-1 data are without turbid water surfaces, and the other two cover large areas of turbid water surfaces, which need special treatment. Before the thin cloud removal, the cut-off frequency for each channel of the images was first determined by the use of the semi-automatic method intro-

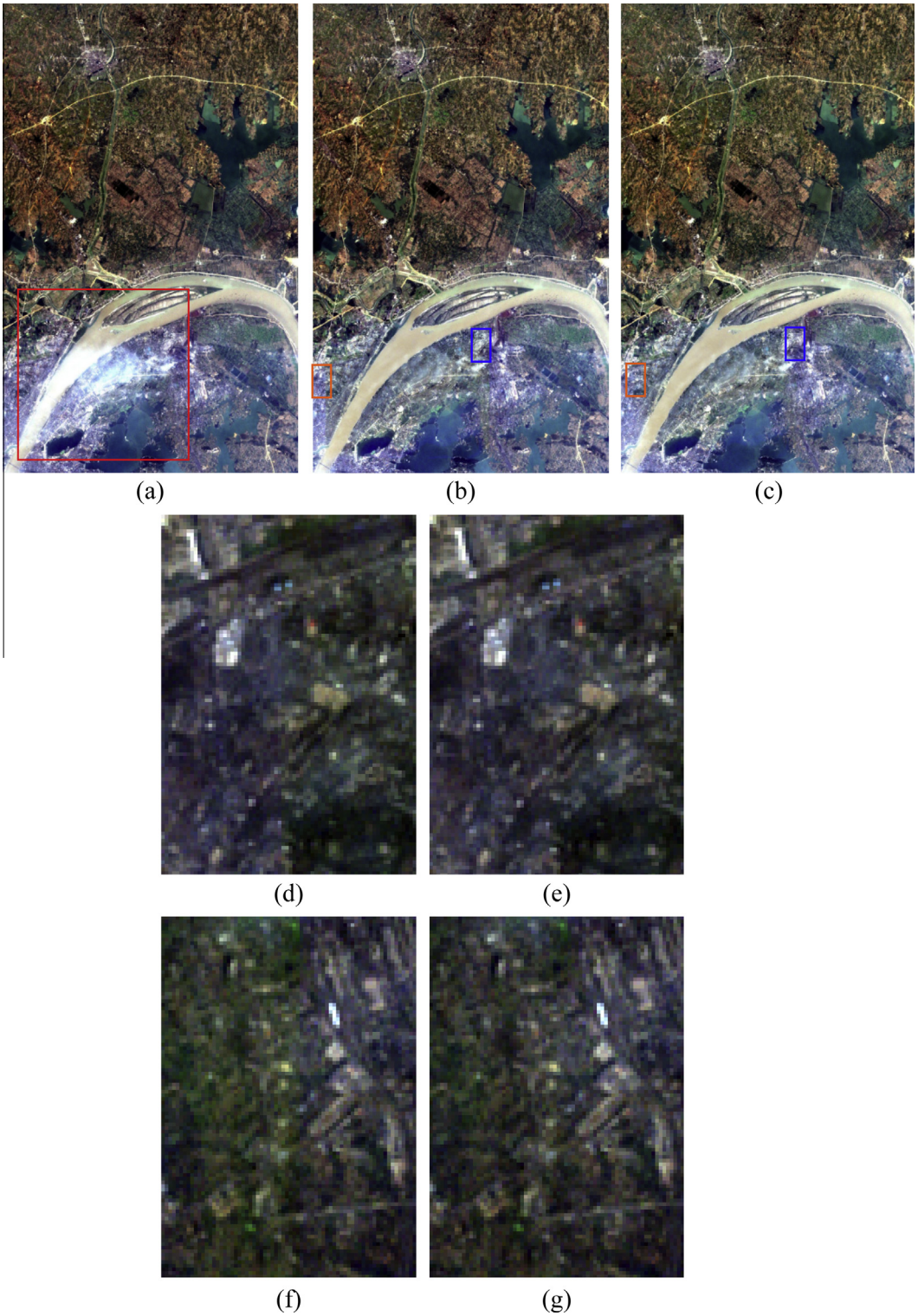

Fig. 9. An example of a large scene by mosaicking the cloudy sub-scenes. (a) The original large scene. (b) The direct mosaicking result. (c) The mosaicking result after removing the seam-lines. (d) and (e) The enlarged region circled by the red rectangle in (b) and (c). (f) and (g) The enlarged region circled by the blue rectangle in (b) and (c). (For interpretation of the references to color in this figure legend, the reader is referred to the web version of this article.)

duced in the methodology section. The results of the proposed method are compared with those of HOT and the traditional HF. Both qualitative and quantitative assessments are performed to evaluate the results.

Fig. 5 shows the three cloudy images without water surfaces and the corresponding thin cloud removal results of HOT, the traditional HF, and the proposed method. To evaluate the thin cloud removal results, two measurements are used: (1) the correction of the cloudy pixels; and (2) the fidelity of the clear pixels. Visually, all of the three methods can remove the thin clouds to a certain degree by correcting the values of the cloudy pixels. However, the color cast is serious in the results of HOT, and the spectra of the clear pixels are changed as well as the cloudy pixels, as the second row of Fig. 5 shows. Since the traditional HF is a global

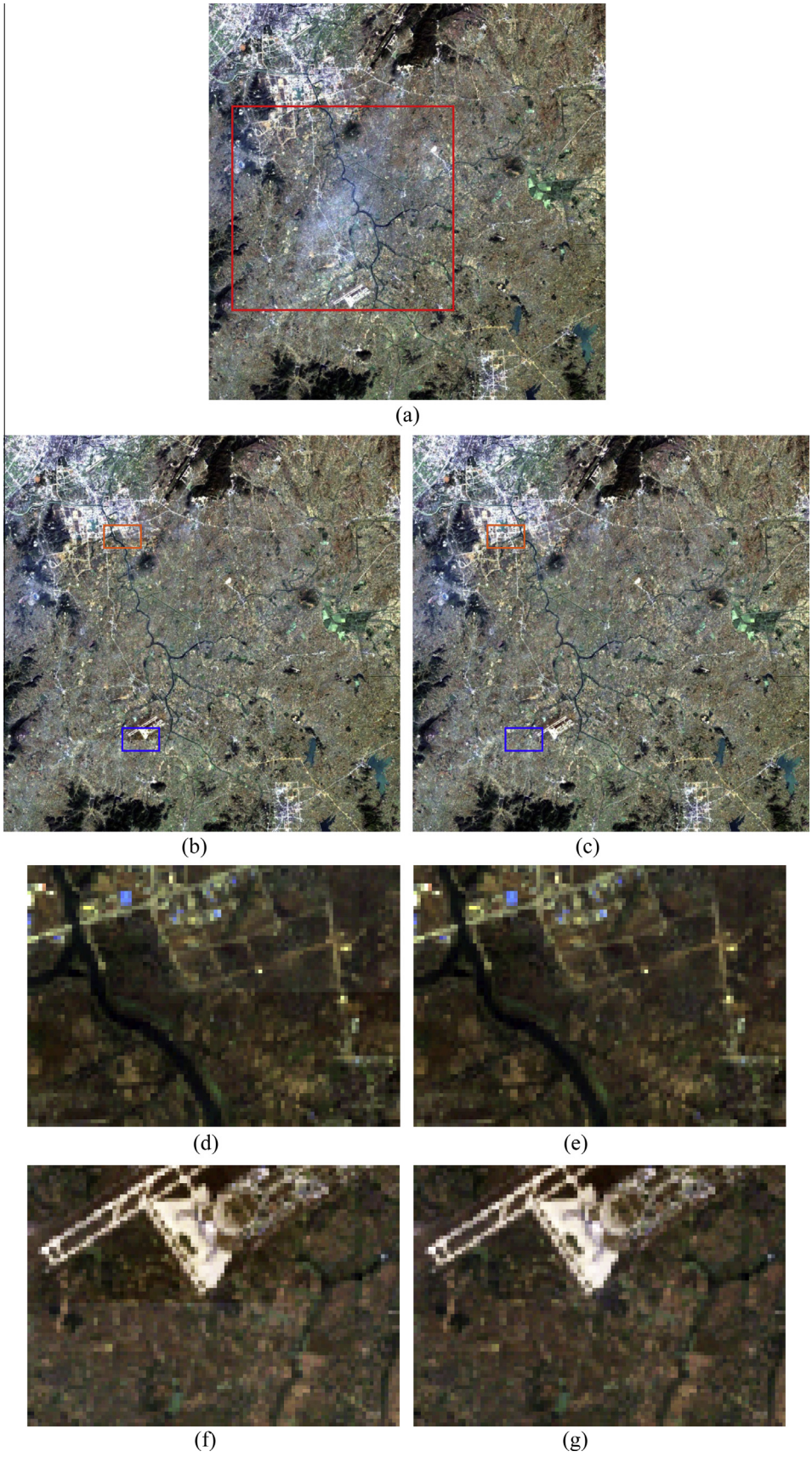

Fig. 10. A further example of a large scene by mosaicking the cloudy sub-scenes. (a) The original large scene. (b) The direct mosaicking result. (c) The mosaicking result after removing the seam-lines. (d) and (e) The enlarged region circled by the red rectangle in (b) and (c). (f) and (g) The enlarged region circled by the blue rectangle in (b) and (c). (For interpretation of the references to color in this figure legend, the reader is referred to the web version of this article.)

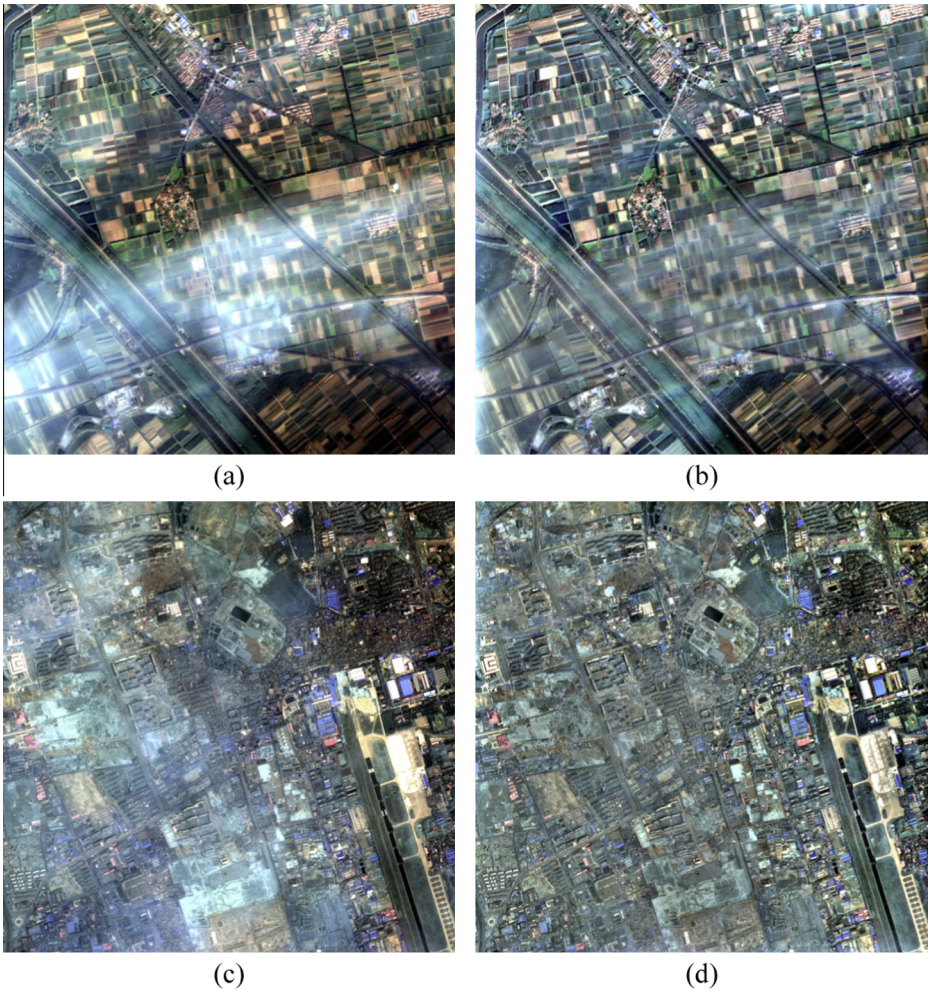

Fig. 11. Results of 2 m spatial resolution data. The first column shows the original thin-cloudy images. The second column shows the corresponding thin cloud removal results of the proposed method.

operation, the values of cloudless pixels in the results of the traditional HF are also changed, as with the HOT results, as shown in the third row of Fig. 5. The general brightness of the results of the traditional HF is darker than those of the original images. Comparing the above results, the results of the proposed method show the natural color by preserving the values of the cloudless pixels, as the last row of Fig. 5 shows.

In order to assess the fidelity of these results quantitatively, we introduce a factor R, which measures the dissimilarity of the cloudless pixels in the results and the original images. R is defined as:

$$R = \frac{\sum |f(x,y) - F(x,y)|}{M}, (x,y) \in \Omega_{cloudless} \quad (11)$$

where $f(x,y)$ and $F(x,y)$ represent the original and resulting images, $\Omega_{cloudless}$ is the set of clear pixels, and M is the number of pixels in $\Omega_{cloudless}$. The smaller the factor R is, the higher the fidelity of the result is. For these three cloudy images, we manually select cloudless samples to compose the cloudless pixel set, as shown in the red[1] polygons in Fig. 6. The values of factor R for the three images and their thin cloud removal results are calculated and listed in Table 2. It can be seen that for all three images, the proposed method results in the smallest value of R in all three of the visible channels. This can be attributed to the cloud identification and the adaptive HF. As the clear and hazy pixels are not treated discriminately in both HOT and the traditional HF, the color cast often appears in the results. Overall, the quantitative evaluation result is consistent with the visual assessment. The conclusion can be made that the proposed locally adaptive thin cloud removal method outperforms the global operations in preserving the fidelity.

Two cloudy images with turbid water surfaces were collected to further evaluate the proposed method. The thin cloud removal results of HOT, the traditional HF, adaptive HF, and the proposed method are shown in Figs. 7 and 8. Parts of the river in Fig. 7 are covered by thin clouds, and the values of the corresponding cloudy pixels are greater than those of the surrounding pixels. It can be observed that the thin clouds are removed in Fig. 7(b), (c), (d), and (e). The tone of Fig. 7(b) is totally different to the original image shown in Fig. 7(a). The values of the cloudy pixels located on the water surface are not properly corrected and they are still higher than the surrounding clear pixels. The HF method maintains the general tone of the original image, as Fig. 7(c) shows, but the values of the cloudless pixels are clearly modified, especially the smooth surfaces of the lakes and the river. The values of the cloudless pixels, such as the lakes located in the bottom-right corner, are preserved by the cloud identification, so that Fig. 7(d) shows a more natural tone than Fig. 7(c). However, the brightness of the river is still very dark in Fig. 7(d), no matter whether the pixels are cloudy or cloudless. In order to improve the result, the water surface preservation step introduced in Section 3 is performed for the river surface in Fig. 7(a). The river surface is first separated from the land surfaces, and it is clustered to three classes: cloudy,

[1] For interpretation of color in Fig. 6, the reader is referred to the web version of this article.

clear, and uncertain, as shown in Fig. 7(e). The values of the cloudy pixels on the river surface are adjusted by Eq. (9) and the result is shown in Fig. 7(f). The average brightness of the river is clearly raised and is close to that of the original cloudless river pixels. Therefore, among the four thin cloud removal results, Fig. 7(f) has the highest fidelity by visual assessment because the values of the cloudless pixels are preserved and the brightness of the turbid water surface is maintained.

Another cloudy image with turbid water surfaces and the corresponding thin cloud removal results are shown in Fig. 8. Among the four thin cloud removal results, Fig. 8(f) shows the most natural color and has the highest fidelity. The same conclusion can be made as for Fig. 7.

The cloudy images (Figs. 7 and 5(a)) are subtracted from the large scenes partially covered by the thin clouds, and are shown in Figs. 9 and 10. The cloudy sub-images are circled by the red rectangles in Figs. 9(a) and 10(a). In practice, in order to obtain the clear large scenes, we need to mosaic the corrected cloud-free sub-images to the original large scenes. The direct mosaicking replaces the cloudy sub-images with the corrected cloud-free sub-images, and the results are shown in Figs. 9(b) and 10(b). Visually, the tones of the direct replacement results are in harmony, without obvious visual disruption. This verifies that the proposed method can yield clear images with high fidelity even though turbid water surfaces are included. However, seam-lines still exist in the boundaries of the cloudy sub-images, as shown in the orange and blue rectangles marked in Figs. 9(b) and 10(b) and the enlarged images shown in Figs. 9(d) and 10(d). Using the strategies described in Section 3, the seam-lines are removed in Figs. 9(c) and 10(c) and the enlarged images shown in Figs. 9(e) and 10(e). It can be seen that clear large scenes without seam-lines are obtained and can be used in the following applications. The seamless mosaicking ensures the applicability of the proposed thin cloud removal method in a large scene.

The above experiments were operated on the medium spatial resolution data. In order to further investigate the application range of the proposed method, two images with 2 meters spatial resolution were employed, which were obtained by China's high definition Earth Observation satellite GaoFen-1, as shown in Fig. 11 (a) and (c). It can be seen that parts of the scenes are contaminated by the thin clouds. Fig. 11(b) and (d) shows the experimental results of the proposed method, in which the radiation of those thin cloudy pixels has been corrected. As the spectral features of the land surfaces are well reserved, the color with high fidelity is exhibited in the thin cloud removal results.

5. Conclusion

An effective and locally adaptive thin cloud removal method is proposed to visible remote sensing data in this paper. The method is limited to remove thin clouds and can result in cloud-free images with high color fidelity. Three stages are included in the proposed method. First, the cut-off frequency for one channel (blue, green or red) is required to be known, which is tuned manually; then the relationship between the gradient and the optimal cut-off frequency is used to determine the cut-off frequencies for other channels semi-automatically. It should be noted that the cut-off frequency varies with the sub-images. Second, the high-fidelity thin cloud removal is achieved by three strategies: (1) thin cloud identification; (2) adaptive HF; and (3) water surface identification and correction. The spectral information of the cloudless pixels is preserved and the brightness of the turbid water surfaces is correctly adjusted. Mosaicking the cloudy sub-images to the original large scene is the final stage of the proposed method, and the seam-lines caused by the direct mosaicking are eliminated in the final cloud-free large scene. In this process, the adjustment length is tuned manually. Experiments on several remote sensing data with medium and high spatial resolutions, including Landsat ETM+ and GaoFen-1 images, validate the effectiveness of the proposed method in efficiently removing thin clouds. Furthermore, the proposed method outperforms HOT and the traditional HF, by both visual and quantitative assessments. All the above results confirm that the proposed method is a simple, effective, and practical thin cloud removal method with significant application potential.

Acknowledgements

This research is Supported by National Natural Science Foundation of China (41271376), Program for New Century Excellent Talents by the Ministry of Education (NCET-10-0648), Wuhan Science and Technology Program (2013072304010825).

References

Ackerman, S.A., Moeller, C.C., Gumley, L.E., Strabala, K.I., Menzel, W.P., Frey, R.A., 1998. Discriminating clear sky from clouds with MODIS. J. Geophys. Res. D: Atmos. 103, 32141–32157.

Chavez Jr., P.S., 1988. An improved dark-object subtraction technique for atmospheric scattering correction of multispectral data. Remote Sens. Environ. 24 (3), 459–479.

Daniel, L., Siong, O.C., Chay, L.S., Lee, K.H., White, J., 2004. A multiparameter moment-matching model-reduction approach for generating geometrically parameterized interconnect performance models. IEEE Trans. Comput. Aided Des. Integr. Circuits Syst. 23 (5), 678–693.

Du, Y., Guindon, B., Cihlar, J., 2002. Haze detection and removal in high resolution satellite image with wavelet analysis. IEEE Trans. Geosci. Remote Sens. 40 (1), 210–217.

Fries, R., Modestino, J., 1979. Image enhancement by stochastic homomorphic filtering. IEEE Trans. Acoust. Speech Signal Process. 27 (6), 625–637.

Gadallah, F., Csillag, F., Smith, E., 2000. Destriping multisensor imagery with moment matching. Int. J. Remote Sens. 21 (12), 2505–2511.

He, X.Y., Hu, J.B., Chen, W., Li, X.Y., 2010. Haze removal based on advanced haze-optimized transformation (AHOT) for multispectral imagery. Int. J. Remote Sens. 31 (20), 5331–5348.

Jensen, J.R., 1996. Introductory Digital Image Processing: A Remote Sensing Perspective, third ed. Prentice-Hall Inc., New Jersey.

Lan, X., Zhang, L., Shen, H., Yuan, Q., Li, H., 2013. Single image haze removal considering sensor blur and noise. EURASIP J. Adv. Signal Process. 2013 (1), 1–13.

Le Hégarat-Mascle, S., André, C., 2009. Use of Markov random fields for automatic cloud/shadow detection on high resolution optical images. ISPRS J. Photogram. Remote Sens. 64 (4), 351–366.

Li, H., Zhang, L., Shen, H., Li, P., 2012. A variational gradient-based fusion method for visible and SWIR imagery. Photogram. Eng. Remote Sens. 78 (9), 947–958.

Li, H., Zhang, L., Shen, H., 2014. A principal component based haze masking method for visible images. IEEE Geosci. Remote Sens. Lett. 11 (5), 975–979.

Liang, S., 2001. Atmospheric correction of landsat ETM+ land surface imagery-part I: methods. IEEE Trans. Geosci. Remote Sens. 39 (11), 2490–2498.

Liu, Z., Hunt, B., 1984. A new approach to removing cloud cover from satellite imagery. Comput. Vis. Graph. Image Process. 25 (2), 252–256.

Maselli, F., Massi, L., Pieri, M., Santini, C., 2009. Spectral angle minimization for the retrieval of optically active seawater constituents from MODIS data. Photogram. Eng. Remote Sens. 75 (5), 595–605.

Perkins, T., Steven, A., Michael, W.M., Alexander, B., Lawrence, S.B., Jamine, L., Marsha, F., 2012. Speed and accuracy improvements in FLAASH atmospheric correction of hyperspectral imagery. Opt. Eng. 51 (11), 111707-1–111707-7.

Poggio, L., Gimona, A., Brown, I., 2012. Spatio-temporal MODIS EVI gap filling under cloud cover: an example in Scotland. ISPRS J. Photogram. Remote Sens. 72 (8), 56–72.

Richter, R., 1996a. Atmospheric correction of satellite data with haze removal including a haze/clear transition region. Comput. Geosci. 22 (6), 675–681.

Richter, R., 1996b. A spatially adaptive fast atmospheric correction algorithm. Int. J. Remote Sens. 17 (6), 1201–1214.

Richter, R., Wang, X., Bachmann, M., Schläpfer, D., 2011. Correction of cirrus effects in Sentinel-2 type of imagery. Int. J. Remote Sens. 32 (10), 2931–2941.

Schreiber, W.F., 1978. Image processing for quality improvement. Proc. IEEE 66 (12), 1640–1651.

Stockham, T.G., 1972. Image processing in the context of a visual model. Proc. IEEE 60 (7), 828–842.

Vermote, E.F., Tanre, D., Deuze, J.L., Herman, M., Morcette, J.-J., 1997. Second simulation of the satellite signal in the solar spectrum: 6S: an overview. IEEE Trans. Geosci. Remote Sens. 35 (3), 675–686.

Zhang, Y., Guindon, B., Cihlar, J., 2002. An image transform to characterize and compensate for spatial variations in thin cloud contamination of Landsat images. Remote Sens. Environ. 82 (2–3), 173–187.